Available online at www.sciencedirect.com
ScienceDirect
Trans. Nonferrous Met. Soc. China 23(2013) 1215−1225
Transactions of Nonferrous Metals Society of China
www.tnmsc.cn

Structural and corrosion characterization of biodegradable Mg−RE (RE=Gd, Y, Nd) alloys

J. KUBÁSEK, D. VOJTĚCH

Department of Metals and Corrosion Engineering, Institute of Chemical Technology, Prague, Technická 5, 166 28 Prague 6, Czech Republic

Received 2 July 2012; accepted 31 October 2012

Abstract: Binary Mg−Gd (up to 5% Gd in mass fraction), Mg−Nd (up to 9% Nd in mass fraction) and ternary Mg−Gd−Y (up to 5% Gd, 1% Y) alloys with precisely determined contents of cathodic impurities (Fe, Ni, Cu, Co) were studied. The alloys were studied in the as-cast state (cooling rate of 500 K/min) and after solution heat treatment (T4). Structures were investigated by optical and scanning electron microscopy, energy dispersive spectrometry, X-ray diffraction and glow discharge spectrometry. Structural investigation was completed by Vickers hardness measurements. Corrosion behavior in the simulated physiological solution (9 g/L NaCl) was assessed by immersion tests and potentiodynamic measurements. It was found that the structures of the as-cast alloys were dominated by fine α-Mg dendrites and eutectic Mg−RE phases. The dendrites exhibited RE-concentration gradients which were most pronounced in the Mg−Gd alloys. For this reason, the T4 heat treatment of the Mg−Gd alloy led to the formation of a new cuboidal Mg_5Gd phase. The corrosion resistance was significantly improved by Gd. The effect of Nd was weak and the addition of Y to Mg−Gd alloys had harmful effect on the corrosion resistance. The T4 heat treatment strongly accelerated the corrosion of Mg−Gd alloys. Its effect on the corrosion of Mg−Nd alloys was not significant. The observed corrosion behavior of the alloys was discussed in relation to their structural states and contents of cathodic impurities.

Key words: biodegradable material; magnesium; rare earths; Mg−RE alloy; structure; corrosion

1 Introduction

Magnesium alloys exhibit high specific strength, good biocompatibility and corrodibility in the human body, making them interesting for biodegradable medical implants, such as orthopaedic fracture fixation devices and cardiovascular stents. Over several decades, researchers have interested in finding Mg-based materials whose strength is sufficiently high to withstand mechanical loading and whose degradation rates are sufficiently low to allow complete healing of the bone defect and to minimize the negative effect of corrosion products of magnesium (hydrogen gas, local increase of pH). For this purpose, many Mg-based alloying systems, such as AZ, AM, AE, ZE, WE, MZ, WZ, LAE, ZK (according to ASTM designation), Mg−Ca, Mg−Zn−Ca, [1−3], have been studied until now. The majority of these alloys were originally developed for engineering applications in the automotive and aerospace industries. Despite hundreds of studies devoted to Mg-based biodegradable alloys, no commercial implants are approved and available at present.

Mg−RE (RE=rare earths) alloys have attracted great interest in recent years as promising candidates for biodegradable implants. From the biocompatibility point of view, RE like gadolinium (Gd) and yttrium (Y) are generally considered relatively acceptable additives in Mg-based alloys, providing that their concentrations are relatively low [4]. Due to anticarcinogenic properties of RE, some authors proposed multifunctional implants based on Mg−RE alloys [5]. For load-bearing applications, such as bone fixation devices, it is important that the implant exhibits sufficient strength and toughness. It is well known that RE elements significantly strengthen magnesium alloys at low or elevated temperatures and improve the elevated temperature creep resistance [6,7]. Significant solid solution strengthening effects were recently observed in Mg−Gd and Mg−Y alloys [8]. Moreover, both Gd and Y show high maximum solid solubility in magnesium (23.5% and 12.5%, respectively [9]) at the eutectic

Corresponding author: J. KUBÁSEK; Tel: +42-0736278401; Fax: +42-0220444400; E-mail: kubasekj@vscht.cz
DOI: 10.1016/S1003-6326(13)62586-8

temperatures. Therefore, additional increase of hardness and strength can be achieved through the T6 heat treatment including solution annealing, quenching and ageing [10]. The strongly positive influence of neodymium on tensile strength at room and elevated temperatures was reported by YAN et al [11].

Apart from the mechanical properties, the corrosion behavior is of great importance in designing biodegradable metallic implants. The corrosion rate of the implant in the human environment should match the rate of healing process of the fractured tissue. In the material engineering community, there is a general agreement that RE improve the corrosion resistance of Mg alloys. The positive effect of RE is attributed to two mechanisms: 1) RE interacts with impurities such as Fe, Ni and Co which are more noble than Mg, and strongly accelerate the galvanic corrosion of Mg alloys. By adding RE, less noble intermetallic phases are created in the structure and galvanic effect is reduced. This behavior is generally referred to as "scavenger effect" [12]. 2) RE atoms incorporate into the surface hydroxide layer, improving its stability and increasing its protective effect against corrosion [12]. Interactions of RE atoms and Cl^- anions are reported to be responsible for this behavior [13].

The corrosion behaviors of Mg−RE alloys have been studied many times, but there are discrepancies between reported results. HORT et al [5] recently studied as-cast binary Mg−Gd alloys containing 2%−15%Gd. They were observed at a minimum corrosion rate of 10%Gd. At higher concentrations, corrosion rate increased, but no explanation was provided. Totally different results were reported by CHANG et al [6] who investigated T6 heat treated Mg−Gd−Y−Zr alloys with 6%−12% Gd. Other alloying elements were kept at constant levels. The alloy with 10%Gd showed the maximum corrosion rate in their work. The corrosion behavior of Mg−Nd alloys was studied by TAKENAKA et al [12] and the positive effect of 1% Nd on the corrosion resistance was found. In contrast, BIRBILIS et al [14] reported that Nd in concentrations from 0.5% to 3.5% worsened the corrosion resistance of Mg−Nd alloys. Studies focused on the influence of T4 and T6 heat treatments on the corrosion resistance of Mg−RE based alloys also provided different results. Some of these studies indicated that the best corrosion resistance corresponded to the T4 state of alloys, followed by the T6 state [15,16]. The worst corrosion resistance was observed for the as-cast alloys in these studies. However, opposite trend was also reported in Ref. [17].

The examples above show that the influence of RE on the corrosion is complicated and it strongly depends on the state and distribution of RE in the structure. In addition, concentrations of impurities (Fe, Ni, Co) in studied alloys are also very important from the corrosion point of view. Unfortunately, in many studies, the influence of impurities is not taken into account. For this reason, this work presents results of the systematic study of as-cast binary Mg−Gd, Mg−Nd and ternary Mg−Gd−Y alloys. The as-cast state was selected because gravity or die casting represents technological alternative to the classical hot extrusion for the production of small implants like screws, plates or nails. The investigated alloys contain RE with high solubility in Mg (Gd, Y) as well as with low solubility (Nd, maximum solid solubility of 3.6% [9]). The study is focused on the relationship between structure and corrosion behavior of the alloys in the simulated physiological solution. In addition, some of the alloys were T4 heat treated to explore the influence of solution annealing on the structure and corrosion behavior.

2 Experimental

In this study, ten alloys were studied in total. They included three binary Mg−Gd alloys, three binary Mg−Nd alloys, three ternary Mg−Gd−Y alloys and pure Mg. Alloy designations and chemical compositions are summarized in Table 1. In chemical analysis of these alloys, we paid great attention to impurities (Fe, Ni, Co, Cu) strongly detrimental to the corrosion resistance. It could be noticed that contents of these impurities are very low except for the Mg−1Gd, Mg−5Gd−1Y and Mg−9Nd alloys containing 180×10^{-6} Ni, 340×10^{-6} Cu and 111×10^{-6} Fe, respectively. It is shown later that this contamination has a direct impact on the corrosion behavior of these alloys.

The Mg−RE alloys were prepared by melting pure magnesium (purity of 99.9%, composition given in Table 1), gadolinium (purity of 99.9%), yttrium (purity of 99.99%) and neodymium (purity of 99%) in a vacuum induction furnace under argon (purity of 99.9%) at ambient pressure to prevent the oxidation of Mg and RE. After 10 min homogenization at 740 °C, the melt was poured into a cast iron metal mold to prepare a cylindrical casting with 50 mm in length and 20 mm in diameter. The average cooling rate was 500 K/min measured by a thermocouple placed in the middle of the mold. The chemical compositions and homogeneity of the castings were verified on both ends of the sample. To determine the effect of RE distribution on the corrosion characteristics of the alloys, the Mg−5Gd and Mg−4Nd alloys were solution heat treated (T4) at 500 °C for 30 h and 520 °C for 20 h, respectively, followed by water quenching. The heat treatment temperatures were optimized according to the Mg−Gd and Mg−Nd phase

Table 1 Alloy designations and chemical compositions of investigated alloys (Excessive contaminations of alloys by harmful impurities are emphasized by bold numbers)

Alloy designation	*w*(Al)/ %	*w*(Si)/ %	*w*(Mn)/ %	*w*(Fe)/ 10^{-6}	*w*(Co)/ 10^{-6}	*w*(Ni)/ 10^{-6}	*w*(Cu)/ 10^{-6}	*w*(Zn)/ %	*w*(Y)/ %	*w*(Nd)/ %	*w*(Gd)/ %	Mg
Pure Mg	0.018	0.045	0.013	10	6	5	6	0.010	−	−	−	Bal.
Mg−1Gd	0.008	0.046	0.032	10	5	180	5	0.009	−	−	0.570	Bal.
Mg−3Gd	0.009	0.062	0.029	11	−	8	8	0.009	−	−	2.845	Bal.
Mg−5Gd	0.007	−	0.011	13	−	3	8	0.007	−	−	4.882	Bal.
Mg−1Nd	0.084	0.021	0.022	24	−	48	21	0.138	−	1.092	−	Bal.
Mg−4Nd	0.022	0.020	−	60	−	6	7	0.025	−	4.359	−	Bal.
Mg−9Nd	−	0.034	−	111	−	5	7	0.015	−	9.261	−	Bal.
Mg−1Gd−1Y	0.009	0.021	0.015	23	−	4	8	0.005	1.020	−	0.629	Bal.
Mg−3Gd−1Y	0.007	−	0.011	36	−	4	13	0.004	0.902	−	3.002	Bal.
Mg−5Gd−1Y	0.006	0.024	0.015	33	−	2	340	0.030	0.892	−	4.763	

diagrams where the eutectic temperatures are 548 °C [9]. In the case of the Mg−4Nd alloy, a slightly higher annealing temperature was applied, because the solid solubility of Nd is lower than that of Gd. The long annealing time was used to ensure the maximum dissolution of the eutectic Mg_5Gd and $Mg_{12}Nd$ phases. The Mg−4Nd alloy was selected for the heat treatment because its Nd-content approaches the maximum solid solubility of Nd in α-Mg (3.6% [9]).

The corrosion behavior of the alloys was studied by immersion tests and potentiodynamic measurements in an aerated simulated physiological solution (9 g/L NaCl). Before the tests, the surface of specimens was modified by grinding on SiC abrasive papers to a final roughness P4000. In the immersion tests, coupons (20 mm in diameter, 2 mm in thickness) were immersed in 250 mL of the solution at 20 °C for 168 h. Corrosion products were removed using a solution of 200 g/L CrO_3, 10 g/L $AgNO_3$ and 20 g/L $Ba(NO_3)_2$, according to ISO 8407. The corrosion rates (mm/a) were calculated using the mass loss measured on a balance with an accuracy of 0.1 mg, according to ASTM G31−72. Each immersion test was performed three times to ensure sufficient statistics. The potentiodynamic curves of the alloys were measured on a potentiostat FAS1 Gamry. Experiments were performed in a standard three-electrode setup: the sample (coupon with 20 mm in diameter and 2 mm in thickness) as the working electrode, platinum wire as counter electrode and Ag/AgCl/KCl (3 mol/L) as the reference electrode (SSCE) with a potential of 0.199 V (vs SHE). Tested area of working electrode was 0.5 cm^2. This area was in contact with 16 mL of 9 g/L NaCl solution. All potentials presented in this work were measured against SSCE. Potentiodynamic curves were scanned from −2.4 V (vs SSCE) to −0.6 V (vs SSCE) at a rate of 2 mV/s.

The structure and elemental distributions of the as-cast and solution heat-treated alloys as well as the corroded surfaces were studied by optical microscopy (OM) and scanning electron microscopy (SEM, Tescan Vega 3) with energy dispersion spectrometry (EDS, Oxford Instruments Inca 350). Prior to the OM and SEM study, the samples were etched with a solution containing 2 mL of nitric acid in 98 mL of ethanol. The phase compositions of the alloys and corrosion products were determined by X-ray diffraction (XRD, X Pert Pro). Concentration profiles of corrosion products were also analyzed by glow discharge spectrometry (GDS, GD Profiler 2, Ar pressure of 650 Pa, source operating at 50 W, approximate sputtering rate of 2.5 μm/min). The structural characterization of the as-cast and T4 heat-treated alloys was completed by Vickers hardness measurements with a loading of 49 N (HV_5).

3 Results

3.1 Structure and hardness

3.1.1 Structure of Mg−Gd and Mg−Gd−Y alloys

Figure 1 shows optical micrographs of the as-cast binary Mg−Gd and ternary Mg−Gd−Y alloys. Except for the Mg−1Gd alloy, structures of all the other materials were similar, containing dendritic patterns typical for the as-cast state. Due to the high cooling rate during casting, dendrites were relatively fine with an average dendrite arm thickness of 20 μm. In the Mg−1Gd alloy, dendrites were not visible and the structure contained only large α-Mg grains because of the low Gd concentration. Similar structure was observed for the pure Mg.

Detailed SEM views of structures are illustrated in Fig. 2. Figure 2(a) shows the structure of the as-cast Mg−5Gd alloy. Similar structure was also observed for the Mg−3Gd alloy. In Fig. 2(a), dendrite cores are depleted in Gd and appear as dark, while dendrite edges

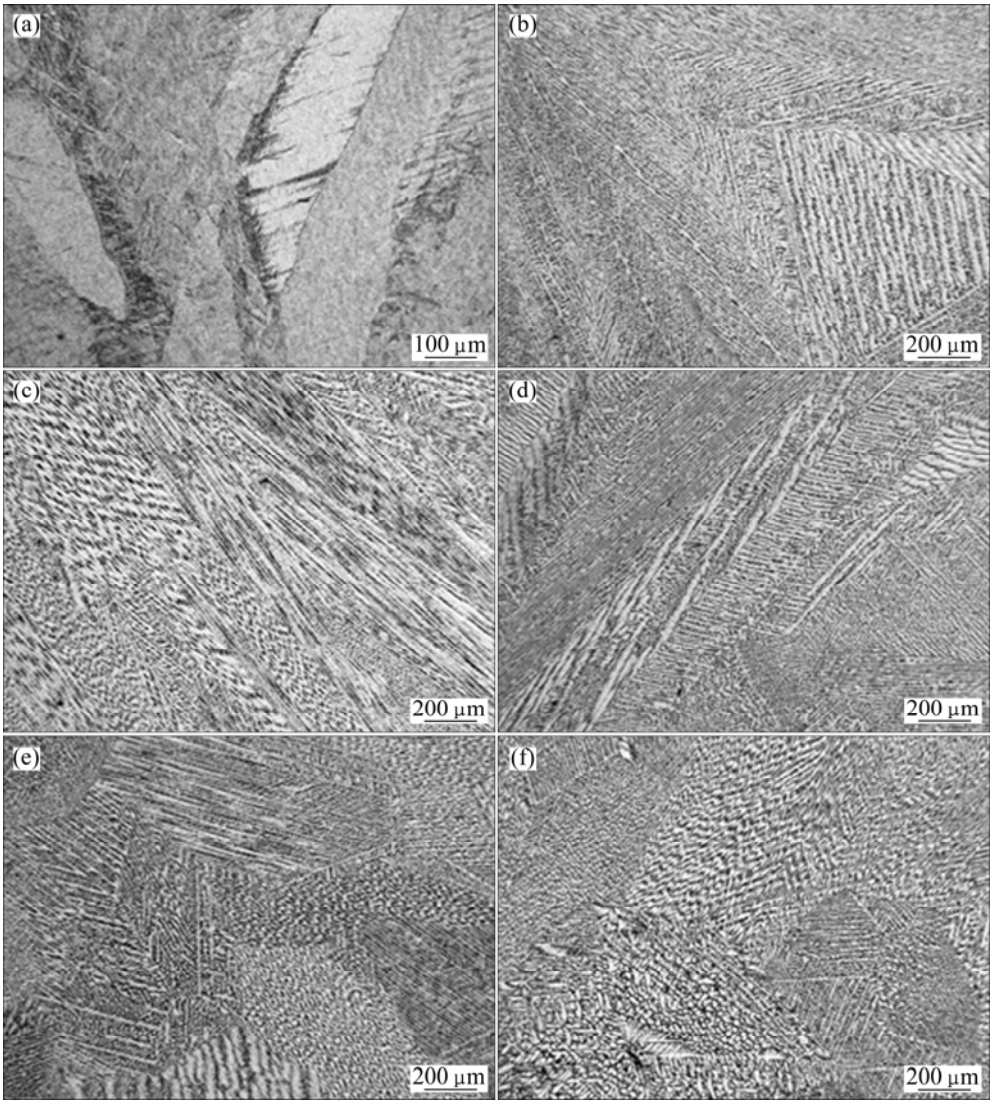

Fig. 1 Optical micrographs of as-cast alloys: (a) Mg−1Gd; (b) Mg−3Gd; (c) Mg−5Gd; (d) Mg−1Gd−1Y; (e) Mg−3Gd−1Y; (f) Mg−5Gd−1Y

are enriched in Gd and are light. Chemical microanalysis was performed to reveal concentration gradients within dendrites. In dendrite cores, the average Gd-content was 2.5%, whereas in dendrite edges it increased up to 21.2% and, perhaps, more. In these regions, light eutectic Mg_5Gd particles were visible, but their volume fraction was low. In the vicinity of Mg_5Gd particles, Gd-content may be higher than the maximum value stated above. The reason is that the measurements in α-Mg phase had to be performed at a minimum distance of approximately 2 μm from the Mg_5Gd particles to prevent the influence of these particles on analysis. Beside the α-Mg and Mg_5Gd phases, there were also small light particles distributed randomly in the structure. Chemical microanalysis revealed the presence of Mg, Gd and O in these particles, so that they correspond to oxides, most probably Gd_2O_3 or $GdMg_2O_4$ [5]. Although melting and casting of the alloys were performed under technical purity (99%) argon, highly reactive Gd could react with oxygen to produce these oxides. The influence of T4 heat treatment on the Mg−5Gd alloy's structure is shown in Fig. 2(b). It is evident that the dendritic microsegregation vanished during the heat treatment. Chemical microanalysis performed at 20 randomly selected points revealed that the average Gd-content in the α-Mg phase was 3.6%. Volume fractions of light particles (oxides and Mg_5Gd) observed in Figs. 2(a) and (b) were measured by an image analyzer. Surprisingly, the light particles in the as-cast alloy occupied (0.30±0.06)%, whereas after the T4 heat treatment their volume fraction increased by three times to (1.00±0.20)%. In addition, the average particle size measured on 1000 particles also increased from 0.6 μm to 0.9 μm. Because binary and ternary oxides are thermally stable phases, it can be assumed that the observed increase of volume fraction and size of light particles is caused by the precipitation and growth of the

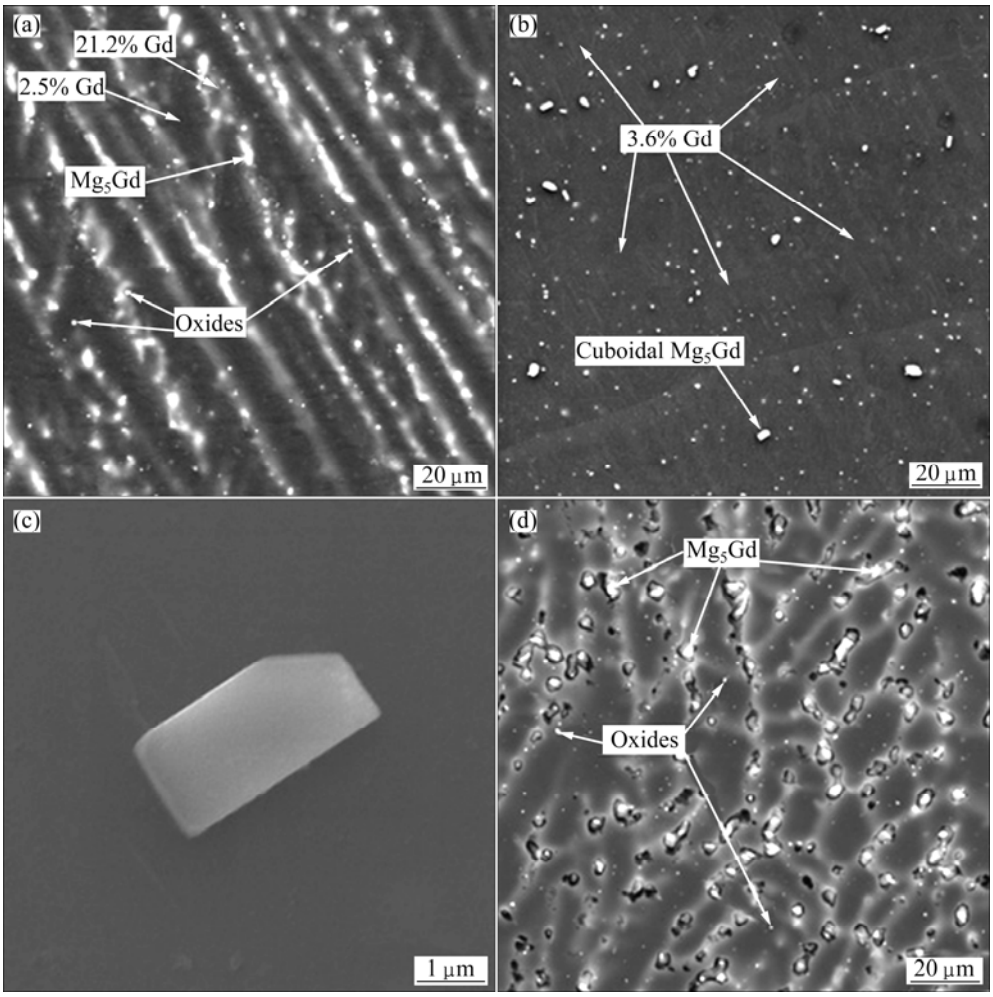

Fig. 2 SEM images of investigated alloys: (a) As-cast Mg−5Gd; (b) T4 heat treated Mg−5Gd; (c) T4 heat treated Mg−5Gd (detailed view); (d) As-cast Mg−5Gd−1Y

Mg_5Gd phase. The newly formed particles are characterized by typical cuboidal shape [6,10], as shown in a detailed view in Fig. 2(c). The chemical composition of this particle was confirmed by EDS analysis. It is discussed later that the formation of new Mg_5Gd particles is a result of the observed Gd content gradients within α-Mg dendrites (Fig. 2(a)) and that it has a strong influence on the corrosion behavior of the alloy.

The SEM image of Mg−Gd−Y alloys is represented in Fig. 2(d) showing the as-cast Mg−5Gd−1Y alloy. The structure was composed of primary α-Mg dendrites (dark), eutectic particles (light) in inter-dendritic regions and small oxide particles (light) distributed randomly. EDS analysis revealed that the eutectic particles corresponded to the Mg_5Gd phase because Y-content in these particles was negligible. EDS also confirmed that all Y was concentrated in α-Mg dendrites. In Fig. 2(d), the amount of eutectic particles is larger than that in the binary Mg−5Gd alloy (Fig. 2(a)) because Y is known to reduce the solid solubility of Gd in the α-Mg phase [18]. The other ternary Mg−Gd−Y alloys had similar structures like that in Fig. 2(d), and only the volume fractions of the eutectic Mg_5Gd phase were lower.

3.1.2 Structure of Mg−Nd alloys

SEM micrographs of the Mg−Nd alloys are shown in Fig. 3. All the alloys contained primary α-Mg dendrites (dark), interdendritic eutectic $Mg_{12}Nd$ phase (light) and small oxidic particles (light). The volume fraction of the eutectic $Mg_{12}Nd$ phase increased with increasing Nd-content. In the Mg−1Nd alloy (Fig. 3(a)), the eutectic phase formed fine separated and almost globular particles. While in the Mg−4Nd alloy, these particles were elongated, branched, but still separated from each other (Fig. 3(b)). A continuous network of the $Mg_{12}Nd$+α-Mg eutectic was visible in the structure of the Mg−9Nd (Fig. 3(c)). Like the Mg−Gd alloys (Fig. 2(a)), the as-cast Mg−Nd alloys were characterized by Nd-content gradients in the α-Mg phase. The concentration differences between dendrite cores and edges were not so large as those in the Mg−Gd alloys, due to the lower maximum solid solubility of Nd (3.6%)

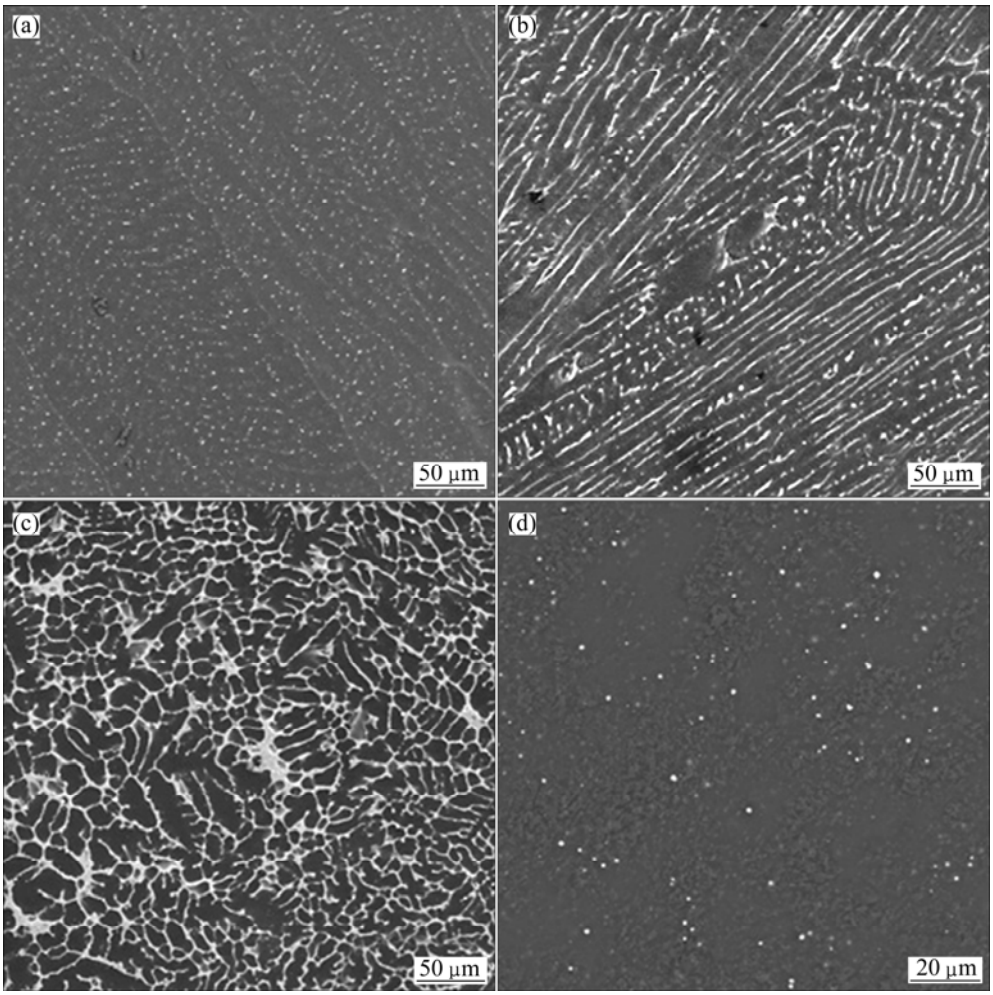

Fig. 3 SEM micrographs of Mg−Nd alloys: (a) As-cast Mg−1Nd; (b) As-cast Mg−4Nd; (c) As-cast Mg−9Nd; (d) T4 heat treated Mg−4Nd

than Gd (23.5%). For example, in the Mg−4Nd alloy, Nd-contents in dendrite cores and edges were 1.2% and 3.8%, respectively (Fig. 3(c)). After the T4 heat treatment of the Mg−4Nd alloy, a large fraction of the interdendritic eutectic $Mg_{12}Nd$ phase vanished (Fig. 3(d)). In addition, microsegregation of Nd also vanished and all the α-Mg phase was characterized by a Nd-content of 2.6%.

3.1.3 Hardness of Mg−RE alloys

The changes of Vickers hardness caused by the additions of Gd, Y and Nd are summarized in Fig. 4. It is evident that the hardness followed the structural development of Mg−RE alloys described above because the hardness increased with increasing contents of alloying elements. It seems that neodymium was slightly more efficient in this way than gadolinium. By adding 4% of Nd, the hardness increased from approximately HVs 30 (pure Mg) to HV_5 53, whereas the addition of 5% of Gd resulted in a hardness of HV_5 47. The combination of Gd and Y led to further increase in hardness. The T4 heat treatment caused a softening of both Mg−5Gd and Mg−4Nd by approximately HV_5 10. Reasons for the observed characteristics are discussed later.

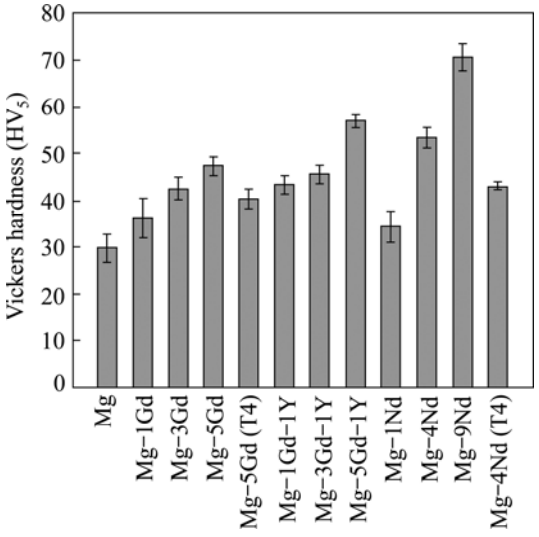

Fig. 4 Vickers hardness (HV_5) of investigated alloys

3.2 Corrosion behavior

3.2.1 Immersion tests

The results of the corrosion immersion tests are summarized for all the investigated alloys in Fig. 5. The following conclusions can be deduced from this figure.

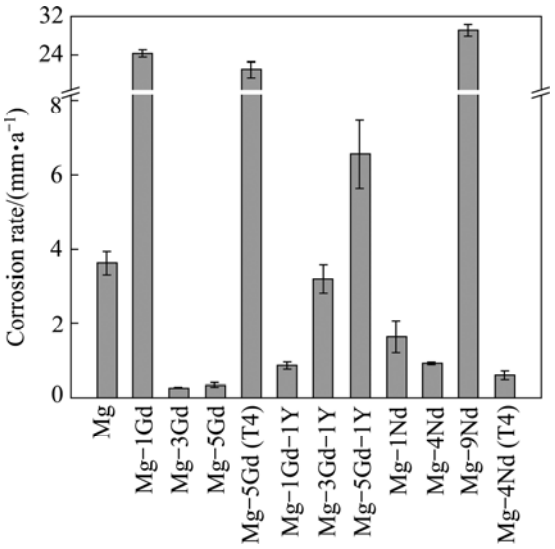

Fig. 5 Corrosion rates of investigated alloys measured by immersion test

1) The addition of Gd improved the corrosion resistance of as-cast alloys compared to the pure Mg. The as-cast Mg−3Gd and Mg−5Gd alloys showed corrosion rates lower than Mg by one order of magnitude, although contents of harmful impurities in all the three alloys were similar. The only exception is the as-cast Mg−1Gd alloy whose corrosion rate achieved more than 20 mm/a. But this increase can be attributed to the contamination of the alloy by nickel (Table 1) whose detrimental effect on the corrosion resistance is well known.

2) The addition of approximately 1% of Y into Mg−Gd alloys resulted in a worsening of the corrosion resistance of as-cast alloys. The Y-addition into the Mg−3Gd alloy led to the tenfold increase of the corrosion rate, while the same Y-addition into the Mg−5Gd alloy increased the corrosion rate almost 20 times. Although the observed acceleration of corrosion attack on the Mg−5Gd−1Y alloy may be partially attributed to its contamination by copper (Table 1), the effect of Y is also significant. The reason is that the content of copper in the alloy (340×10^{-6}) was only slightly above the upper limit recommended to ensure the optimum corrosion performance of Mg-based alloys (300×10^{-6}) [19].

3) The additions of 1% and 4% of Nd caused approximately twofold and threefold decrease of the corrosion rate, respectively, compared to the pure Mg. Therefore, the effect of Nd in these contents was less pronounced than that of Gd. However, when adding 9% of Nd, a strong acceleration of the corrosion process was observed. The corrosion rate of the Mg−9Nd alloy is 29 mm/a, i.e., almost eightfold that of the pure Mg. The contamination of this alloy by 111×10^{-6} of iron may play a role in this acceleration, but the structural state of the alloy is also important (see Discussion part).

4) The T4 heat treatment of the Mg−5Gd alloy had a strongly detrimental influence on the corrosion resistance. The corrosion rate increased from 0.4 mm/a to 21 mm/a due to the heat treatment.

5) In contrast to the Mg−Gd system, the T4 heat treatment applied to the Mg−4Nd alloy improved the corrosion resistance, but only slightly. The as-cast alloy showed the corrosion rate of 0.9 mm/a, while its T4 heat treated counterpart corroded at a rate of 0.6 mm/a. Due to possible experimental error of the immersion technique, this difference is not significant.

3.2.2 Potentiodynamic measurements

Potentiodynamic curves are shown in Fig. 6 and corrosion parameters are summarized in Table 2. Figure 6(a) which compares the as-cast Mg, Mg−5Gd and Mg−5Gd−1Y alloys indicates that the addition of gadolinium shifted the corrosion potential to higher values, i.e., it increased the nobility of magnesium (see also Table 2). It is in accordance with the slightly more noble natures of Mg−RE phases compared with magnesium [20]. It was observed that gadolinium forms the Mg_5Gd phase in the structure (Figs. 1 and 2). Moreover, comparing the Mg and Mg−5Gd alloys in Table 2, one can see that the corrosion current density was also reduced due to the gadolinium. The observed trends in both corrosion potential and current density caused by gadolinium are consistent with the changes of corrosion rates determined by the immersion tests (Fig. 5). It is also seen in Fig. 6(a) and Table 2 that the addition of 1% of Y to the Mg−5Gd alloy did not influence the measured corrosion parameters significantly. The influence of T4 heat-treatment on the potentiodynamic curves of the Mg−5Gd alloy is illustrated in Fig. 6(b). It is evident that the heat treatment slightly increased the corrosion potential from −1.74 to −1.65 V (vs SSCE). The reason may be in the formation of cuboidal Mg_5Gd particles during the heat treatment (Fig. 2) which are more noble than Mg matrix. The heat treatment also led to an increase of the corrosion current density from 13×10^{-3} to 33×10^{-3} mA/cm^2, which is in agreement with the increased corrosion rate of the heat-treated alloy in the simulated physiological solution (Fig. 5). The influence of Nd on potentiodynamic curves is illustrated in Fig. 6(c). The corrosion potential of the as-cast alloys increased with increasing amount of Nd due to the formation of the more noble eutectic $Mg_{12}Nd$ phase in the structure (Fig. 3). Corrosion current density first decreased with

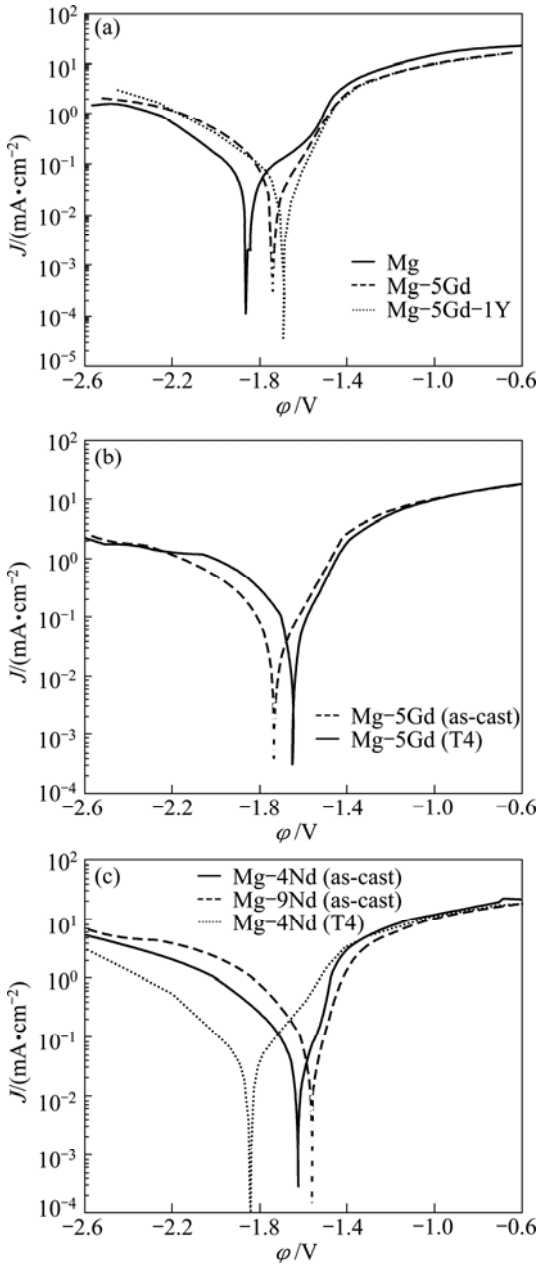

Fig. 6 Potentiodynamic curves of investigated alloys: (a) Influence of Gd and Y; (b) Influence of T4 heat-treatment of Mg−5Gd alloy; (c) Influence of Nd and T4 heat-treatment of Mg−4Nd alloy

Nd-additions up to 4%, followed by its increase at 9% of Nd. This trend was similar to the behavior of Mg−Nd alloys during the immersion tests (Fig. 5). The T4 heat treatment influenced the corrosion potential of the Mg−4Nd alloy differently from the Mg−5Gd. As it is shown in Fig. 3, a large fraction of the eutectic phase was dissolved in the α-Mg solid solution during the heat treatment. Therefore, there was a clear shift of the corrosion potential to a more negative value of −1.84 V (vs SSCE) close to that of the pure Mg (Fig. 6(c), Table 2).

Table 2 Corrosion parameters of as-cast and T4 heat-treated alloys (φ_C-corrosion potential, J-corrosion current density) determined from potentiodynamic curves

Alloy	φ_C (vs SSCE)/V	J/(μA·cm^{-2})
Mg (as-cast)	−1.88	23
Mg−1Gd (as-cast)	−1.74	27
Mg−3Gd (as-cast)	−1.74	23
Mg−5Gd (as-cast)	−1.74	13
Mg−5Gd (T4)	−1.65	33
Mg−1Nd (as-cast)	−1.63	11
Mg−4Nd (as-cast)	−1.62	9
Mg−4Nd (T4)	−1.84	18
Mg−9Nd (as-cast)	−1.56	20
Mg−1Gd−1Y (as-cast)	−1.64	24
Mg−3Gd−1Y (as-cast)	−1.68	25
Mg−5Gd−1Y (as-cast)	−1.69	14

4 Discussion

4.1 Influence of RE on structure and hardness

Due to the rapid cooling of the Mg−RE alloys during casting, their structures correspond to the non-equilibrium solidification. One consequence of the rapid solidification is the presence of RE-concentration gradients in primary α-Mg dendrites. These gradients are steeper in the Mg−Gd alloys than in the Mg−Nd alloys due to the high solid solubility of Gd in Mg. In the Mg−5Gd alloy (Fig. 2(a)), the maximum Gd-content in the α-Mg phase even approaches the maximum solid solubility of 23.5% at 548 °C [9], although the total Gd-content in the alloy is significantly lower (4.9%). It is likely that regions in the α-Mg phase which are strongly saturated with Gd are prone to decompose at elevated temperatures, i.e., during the T4 heat treatment. The decomposition occurs both by the growth of the existing eutectic Mg_5Gd particles and by the formation of new cuboidal particles (Figs. 2(b) and (c)). The average Gd-content in the α-Mg phase thus significantly decreases. The formation of new cuboidal Mg_5Gd phase during T4 heat treatments of Mg−Gd-based alloys was reported also by other authors [6,10].

When Y is added to Mg−Gd alloys, it reduces the solid solubility of Gd in Mg [18]. Therefore, the ternary Mg−Gd−Y alloys contain larger volume fractions of the Mg_5Gd intermetallic phase compared to the binary Mg−Gd alloys with the same Gd amount (Fig. 2(d)). Yttrium remains dissolved in the α-Mg solid solution. The absence of $Mg_{24}Y_5$ intermetallic phase in the structures of the Mg−Gd−Y alloys is accounted for by the low concentration of Y and by the fact that this phase forms at low temperatures of approximately 270 °C [18] at which diffusivity of Y is low. Relatively rapid cooling

during the casting process prevents the formation of the new $Mg_{24}Y_5$ phase. The as-cast Mg−4Nd alloy behaves differently from the Mg−5Gd during the heat treatment. This alloy contains the eutectic $Mg_{12}Nd$ phase which partly dissolves in the α-Mg solid solution during the solution heat treatment (Fig. 3). In this alloy, the driving force for the formation of new $Mg_{12}Nd$ particles is low due to the low Nd-concentration and Nd-concentration gradients in dendrites.

The observed development of hardness with additions of RE (Fig. 4) reflects two main hardening mechanisms: 1) hardening by hard secondary eutectic phases (Mg_5Gd and $Mg_{12}Nd$); 2) solid solution hardening by RE dissolved in the α-Mg phase.

Hall-Petch hardening caused by dendrite or grain boundaries is not affected by RE because the dendrite size is similar for all the investigated Mg−RE alloys (Figs. 1 and 3). In the Mg−Gd alloys, the volume fraction of the eutectic Mg_5Gd phase is low (Fig. 2(a)), so the main hardening contribution is solid solution hardening by large Gd atoms inducing an internal elastic stress in the α-Mg lattice. The α-Mg phase contains even more that 20% of Gd in the Mg−5Gd alloy (Fig. 2(a)). The addition of 1% of Y supports the formation of Mg_5Gd phase and, therefore, leading to additional increase of hardness (Fig. 4). By T4 heat treatment of the Mg−5Gd alloy, the hardness is slightly reduced because the average Gd content in the α-Mg phase is reduced. It is associated with the formation of the new cuboidal Mg_5Gd particles (Fig. 2). In the Mg−Nd alloys, the contribution of the hard eutectic phase (Fig. 3) to the observed hardness is more significant due to the lower Nd solubility in Mg. The T4 heat treatment of the Mg−4Nd alloy also leads to softening. The reason is that the hard eutectic $Mg_{12}Nd$ phase dissolves in magnesium matrix (Fig. 3(d)). The effect of solid solution hardening is small due to the low Nd-content in α-Mg after the T4 heat treatment (2.6%).

4.2 Influence of RE on corrosion behavior

It is evident from Figs. 5, 6 and Table 2 that gadolinium positively influences the corrosion resistance of Mg-based alloys. The Mg−5Gd and Mg−3Gd alloys are characterized by significantly lower corrosion rates in the simulated physiological solution than pure magnesium. Comparing the contents of Fe, Ni and Cu impurities in these Mg−Gd alloys and in Mg, one can see that these contents are very similar. Therefore, the "scavenger effect" is not responsible for this behavior. The XRD analysis of corrosion products on Mg−Gd alloys (not shown) reveals that they contain only magnesium hydroxide phase. Gadolinium oxides or hydroxides are not detected. However, a more detailed elemental profiling analysis of the surface layer performed by GDS (Fig. 7) indicates that gadolinium is incorporated to the magnesium hydroxide layer where Gd^{3+} cations substitute Mg^{2+} cations in the brucite lattice. The corrosion behavior of magnesium alloys depends on the protective effect of the surface hydroxide-based corrosion products and gadolinium evidently supports this protective effect. One explanation may be that Gd^{3+} cations locally increase positive charge in the brucite lattice. This increase is balanced by interaction of Gd^{3+} cations with Cl^- anions, which slows down the penetration of harmful Cl^- anions through the hydroxide layer to the metallic substrate. The corrosion resistance of the as-cast Mg−3Gd and Mg−5Gd alloys is also supported by the fact that the main portion of Gd in these alloys is concentrated in the α-Mg solid solution (Fig. 2). The volume fraction of the more noble Mg_5Gd eutectic phase is very low in these alloys, moreover, this phase is surrounded by a strongly Gd-enriched α-Mg phase. Therefore, the contribution of Mg_5Gd to the galvanic corrosion is small.

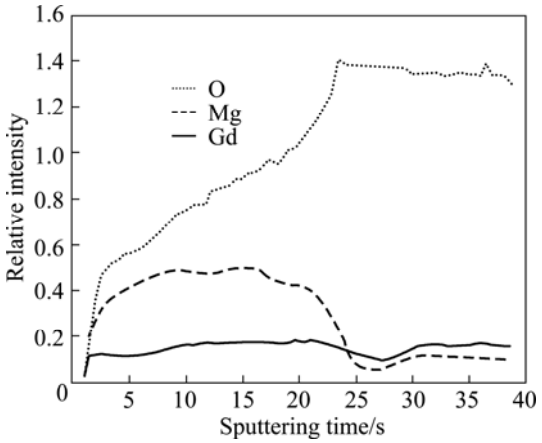

Fig. 7 GDS elemental profiles in surface of corroded Mg−5Gd alloy

The influence of T4 heat treatment on the corrosion resistance of the Mg−5Gd alloy is strongly detrimental (Fig. 5). It can be assumed that the structural changes induced by the heat treatment are responsible for this behavior. As is shown in Fig. 2, these structural changes include the formation of new Mg_5Gd particles and a strong depletion of the surrounding α-Mg phase in Gd. Both factors strongly accelerate the galvanic corrosion. Moreover, approximately 30 Mg_5Gd particles were analyzed by EDS both in the as-cast Mg−5Gd alloy and the T4 heat treated one to explain the observed behavior. Surprisingly, an increase of Cu content in some of the analyzed particles was detected after the heat treatment. In the as-cast Mg−5Gd alloy, the Cu-content in all analyzed particles was below the EDS detection limit (approximately 0.1%), whereas after the heat treatment there were a few particles containing up to 0.4% of Cu. It

can be assumed that this change increases the nobility of Mg_5Gd particles, which may be another contribution to the observed acceleration of the corrosion after the T4 heat treatment.

Figure 5 indicates that the addition of 1% of yttrium to the Mg−Gd alloys accelerates the corrosion process. Apparently, the reason is in an increased volume fraction of the eutectic Mg_5Gd phase due to yttrium (Fig. 2). This phase is more noble than the α-Mg matrix and accelerates the galvanic corrosion of the alloys.

The influence of neodymium on the corrosion behavior depends on its content. At Nd-contents of 1% and 4%, the effect of Nd on the corrosion resistance is positive (Fig. 5, Table 2). As is proved by GDS (not shown), the reason is similar to that of Gd, namely, neodymium incorporates to the surface hydroxide layer and hinders the diffusion of Cl^- through this layer towards the metal. However, neodymium has a lower solid solubility in magnesium than gadolinium, therefore, the Mg−Nd alloys contain significantly higher volume fractions of eutectic phase (compare Figs. 2 and 3). For this reason, the galvanic corrosion plays a more significant role in the as-cast Mg−Nd alloys than in the Mg−Gd alloys and the positive effect of Nd on the corrosion is thus weaker compared to Gd. Different situation is observed in the case of the Mg−9Nd alloy. This alloy corroded at a considerably higher rate compared to both Mg and other Mg−Nd alloys. This behavior can be attributed to two factors: 1) The Mg−9Nd alloy is contaminated by 111×10^{-6} of Fe (Table 1); 2) Unlike the Mg−1Nd and Mg−4Nd alloys, the Mg−9Nd alloy contains the continuous network of the eutectic $Mg_{12}Nd$ phase (Fig. 3(c)). This network represents a good path for the fast localized galvanic corrosion. It is illustrated in Fig. 8 that the corrosion occurs in the α-Mg phase in the vicinity of the eutectic phase. When the eutectic phase is discontinuous (the Mg−1Nd and Mg−4Nd alloys, Fig. 8(a)), the corrosion process is not severe, corrosion pits separated from each other are observed after removing corrosion products, and the alloy retains its compactness. However, in the case of a continuous network of the eutectic phase (the Mg−9Nd alloy, Fig. 8(b)), the corrosion attack breaks down the material's compactness and large fragments are rapidly detached from the material.

In contrast to the Mg−5Gd alloy, the influence of the T4 heat treatment on the corrosion resistance of Mg−4Nd alloy is positive (Fig. 5). The structural investigation revealed that the heat treatment induced a partial dissolution of the eutectic $Mg_{12}Nd$ phase in the Mg solid solution (Fig. 3(d)). For this reason, the galvanic corrosion is suppressed, but this effect is not very significant because it only leads to a decrease of the corrosion rate from 0.9 to 0.6 mm/a.

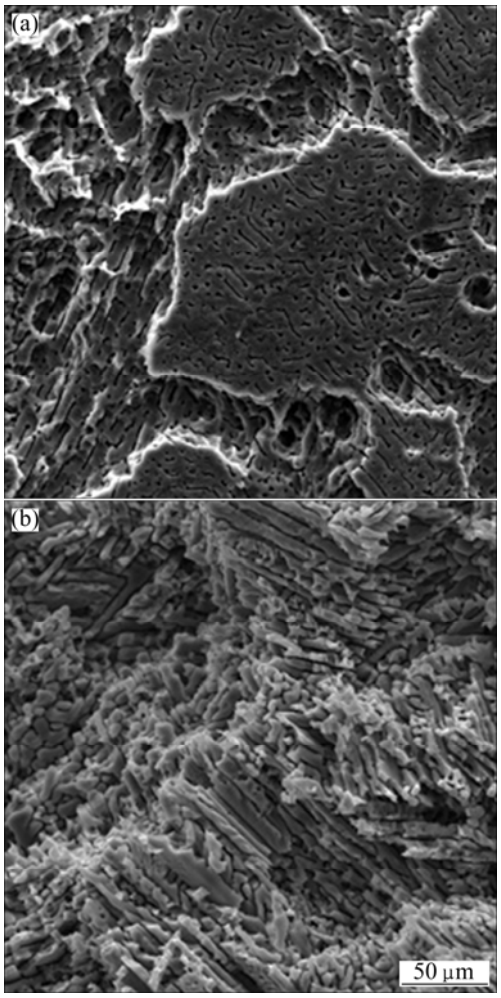

Fig. 8 SEM images showing surface morphologies of Mg−4Nd (a) and Mg−9Nd (b) alloys after 318 h corrosion in simulated physiological solution and chemical removing of corrosion products by pickling in solution of 200 g/L CrO_3, 10 g/L $AgNO_3$ and 20 g/L $Ba(NO_3)_2$, according to ISO 8407

5 Conclusions

1) Both Gd and Nd improve the corrosion resistance of as-cast Mg-based alloys. The influence of Gd is more pronounced, because it has a higher solid solubility in Mg than Nd, and because Mg−Gd alloys contain lower fractions of cathodic eutectic phases.

2) The effect of Gd is significant despite very low concentrations of cathodic impurities like Fe, Ni and Cu, suggesting that an improvement of the protective effect of the surface hydroxide layer by Gd accounts for this behavior.

3) Additions of Y to Mg−Gd alloys support the formation of Mg_5Gd eutectic phase and, therefore, accelerate the galvanic corrosion.

4) The solution heat treatment of the Mg−5Gd alloy negatively influences the corrosion resistance. The reason is the formation of new cuboidal cathodic Mg_5Gd

phase, depletion of the α-Mg phase by Gd and, perhaps, redistribution of impurities in the alloy.

Acknowledgements

The authors would like to thank the Czech Science Foundation (P108/12/G043) and the Academy of Sciences of the Czech Republic (KAN300100801) for the financial support.

References

[1] ZENG R C, DIETZEL W, WITTE F, HORT N, BLAWERT C. Progress and challenge for magnesium alloys as biomaterials [J]. Advanced Engineering Materials, 2008, 10(8): B3−B14.

[2] WITTE F. The history of biodegradable magnesium implants: A review [J]. Acta Biomaterialia, 2010, 6(5): 1680−1692.

[3] VOJTĚCH D, ČÍŽOVÁ H, VOLENEC K. Investigation of magnesium-based alloys for biomedical applications [J]. Metallic Materials, 2006, 44: 211−223.

[4] XIN Y, HU T, CHU P K. In vitro studies of biomedical magnesium alloys in a simulated physiological environment: A review [J]. Acta Biomaterialia, 2011, 7(4): 1452−1459.

[5] HORT N, HUANG Y, FECHNER D, STORMER M, BLAWERT C, WITTE F. Magnesium alloys as implant materials—Principles of property design for Mg−RE alloys [J]. Acta Biomaterialia, 2010, 6(5): 1714−1725.

[6] CHANG J, GUO X, HE S, FU P, PENG L, DING W. Investigation of the corrosion for Mg–*x*Gd–3Y–0.4Zr (*x*=6, 8, 10, 12wt%) alloys in a peak-aged condition [J]. Corrosion Science, 2008, 50(1): 166−177.

[7] ROKHLIN L L, NIKITINA N I. Recovery after ageing of Mg−Y and Mg−Gd alloys [J]. Journal of Alloys and Compounds, 1998, 279(2): 166−170.

[8] GAO L, CHEN R S, HAN E H. Effects of rare-earth elements Gd and Y on the solid solution strengthening of Mg alloys [J]. Journal of Alloys and Compounds, 2009, 481(1−2): 379−384.

[9] GALE W F, TOTEMEIER T C. Smithells metals reference book [M]. 8th ed. Oxford: Elsevier Publishers, 2004: 2080.

[10] HE S M, ZENG X Q, PENG L M, GAO X, NIE J F, DING W J. Microstructure and strengthening mechanism of high strength Mg−10Gd−2Y−0.5Zr alloy [J]. Journal of Alloys and Compounds, 2007, 427(1−2): 316−323.

[11] YAN J, SUN Y, XU F, XUE S, TAO W. Microstructure and mechanical properties in cast magnesium–neodymium binary alloys [J]. Materials Science and Engineering A, 2008, 476(1−2): 366−371.

[12] TAKENAKA T, ONO T, NARAZAKI Y, NAKA Y, KAWAKAMI M. Improvement of corrosion resistance of magnesium metal by rare earth elements [J]. Electrochimica Acta, 2007, 53(1): 117−121.

[13] YAO H B, LI Y, WEE A T S, PAN J S, CHAI J W. Correlation between the corrosion behavior and corrosion films formed on the surfaces of $Mg_{82-x}Ni_{18}Nd_x$ (*x*=0, 5, 15) amorphous alloys [J]. Applied Surface Science, 2001, 173(1−2): 54−61.

[14] BIRBILIS N, EASTON M A, SUDHOLZ A D, ZHU S M, GIBSON M A. On the corrosion of binary magnesium-rare earth alloys [J]. Corrosion Science, 2009, 51(3): 683−689.

[15] LIANG S Q, GUAN D K, TAN X P. The relation between heat treatment and corrosion behavior of Mg−Gd−Y−Zr alloy [J]. Materials & Design, 2011, 32(3): 1194−1199.

[16] PENG L M, CHANG J W, GUO X W, ATRENS A, DING W J, PENG Y H. Influence of heat treatment and microstructure on the corrosion of magnesium alloy Mg−10Gd−3Y−0.4Zr [J]. Journal of Applied Electrochemistry, 2009, 39(6): 913−920.

[17] CHANG J, GUO X, HE S, FU P, PENG L, DING W. Investigation of the corrosion for Mg–*x*Gd–3Y–0.4Zr (*x*=6, 8, 10, 12wt%) alloys in a peak-aged condition [J]. Corrosion Science, 2008, 50(1): 166−177.

[18] GUO Y, LI J, LI J, YANG Z, ZHAO J, XIA F, LIANG M. Mg–Gd–Y system phase diagram calculation and experimental clarification [J]. Journal of Alloys and Compounds, 2008, 450(1−2): 446−451.

[19] ATRENS A, LIU M, ABIDIN N I Z. Corrosion mechanism applicable to biodegradable magnesium implants [J]. Materials Science and Engineering B, 2011, 176(20): 1609−1636.

[20] COY A E, VIEJO F, SKELDON P, THOMPSON G E. Susceptibility of rare-earth-magnesium alloys to micro-galvanic corrosion [J]. Corrosion Science, 2010, 52(12): 3896−3906.

可生物降解 Mg−RE (RE=Gd, Y, Nd) 合金的组织与腐蚀性能

J. KUBÁSEK, D. VOJTĚCH

Department of Metals and Corrosion Engineering, Institute of Chemical Technology,

Prague, Technická 5, 166 28 Prague 6, Czech Republic

摘　要：对含有确定杂质(Fe, Ni, Cu, Co)成分的二元 Mg−Gd (<5% Gd，质量分数)、Mg−Nd(<9% Nd)合金和三元 Mg−Gd−Y(<5% Gd, 1% Y)合金的显微组织与腐蚀性能进行研究。所研究合金为铸态(冷却速率 500 K/min)或 T4 固溶热处理态。采用光学显微镜、扫描电子显微镜、能谱仪、X 射线衍射和辉光放电光谱法对合金进行表征，采用维氏硬度仪测量其硬度。通过在 9 g/L NaCl 模拟生理溶液中的浸泡试验和动电位测试研究其腐蚀性能。结果表明，铸态合金的显微组织以细小的 α-Mg 枝晶和 Mg−RE 共晶为主。Mg−Gd 合金中的枝晶存在明显的稀土浓度梯度。为此，对 Mg−Gd 合金进行 T4 热处理，以形成新的立方 Mg_5Gd 相。添加 Gd 后合金的抗腐蚀性能得到明显改善，添加 Nd 的影响较微弱，而添加 Y 对 Mg−Gd 的抗腐蚀性有不利影响。T4 热处理显著地加快了 Mg−Gd 合金的腐蚀，但对 Mg−Nd 合金的影响不明显。对合金的腐蚀行为与显微组织和所含杂质的关系进行了讨论。

关键词：生物降解材料；镁；稀土；Mg−RE 合金；组织；腐蚀

(Edited by Hua YANG)